Electrothermal modeling for nano AlGaN/GaN HEMTs using dual-phase-lag theory

Randa Khemiri
University of Monastir: Universite de Monastir
Mohamed Hichem Gazzah (hichem.gazzah@fsm.rnu.tn)
University of Monastir: Universite de Monastir https://orcid.org/0000-0003-4816-8374
Hafedh Belmabrouk
University of Majmaah

Research Article

Keywords: AlGaN/GaN HEMTs, DPL model, 2DEG Density, thermal flux, Heat generation.

Posted Date: February 22nd, 2021

DOI: https://doi.org/10.21203/rs.3.rs-162221/v1

Electrothermal modeling for nano AlGaN/GaN HEMTs using dual-phase-lag theory

Randa Khemiri[1], Mohamed Hichem Gazzah[2] and Hafedh Belmabrouk[1]

[1]Electronics and Microelectronics Laboratory, Faculty of Sciences of Monastir, University of Monastir, Monastir 5019, Tunisia, e-mail: randa.khemiri@gmail.com

[2]Quantum and Statistical Physics Laboratory, Faculty of Sciences of Monastir, University of Monastir, Monastir 5019, Tunisia, e-mail: hichem.gazzah@fsm.rnu.tn

Abstract– The combined dependence of the electronic and thermal characteristics in the AlGaN/GaN HEMTs supported in nano-elctronic devices was studied theoretically and numerically. The Schrödinger-Poisson equations coupled with Dual phase lag (DPL) thermal transfer equation was undertaken. Simultaneous impacts of the conduction band offset and polarization charge between the AlGaN/GaN heterointerface induce the production of the two-dimensional electron gas density (2DEG). The simulation results showed that the 2DEG density at the heterointerface increased with increase of Aluminum fraction. In addition, the simulation results of the thermalization process were found to be in good agreement with the literature. As a result, the maximum heat generation as well the maximum temperature at the heterointerface increased. The obtained result could to be useful in assessing thermal transfer in the AlGaN/GaN HEMTs nano-devices to improve their performance.

Keywords – AlGaN/GaN HEMTs; DPL model; 2DEG Density; thermal flux; Heat generation.

1. Introduction

High Electron Mobility Transistors (HEMTs) power components on Gallium Nitride (GaN) have demonstrated their potential to respond to high frequency applications such as radar, space or telecommunications. Up to now the best performances of HEMTs AlGaN/GaN transistors in terms of current cutoff frequency (f_t=454GHz) and in power (f_{max}=444GHz) have been obtained for 20 nm long gates [1]. The increase in the frequency of components, linked to their miniaturization, is inevitably accompanied by an increase in the power dissipated, causing significant self-heating.

Several ways are being studied to improve the thermal dissipation of transistors in the GaN industry. The substrate used for the growth of the AlGaN/GaN heterostructure must have good electrical resistivity and good thermal conductivity to promote heat dissipation from

operating components [2-4]. A new and growing voice for improving the cooling of electronic circuits is to integrate micro-channels directly into the circuits allowing the circulation of water and ensuring the cooling of the components [5].

Thus, it has been demonstrated that the management of the thermal dissipation of the components is a major stake in obtaining reliable electronic systems. In order to optimize the thermal management of components, it is important to know the operating temperature of components in real time. The real-time knowledge of this temperature allows control and ensure preventive and non-curative maintenance of electronic systems.

The answer projected by several works considers the temperature as an external parameter as close as possible to their hot point close to the maximum operating temperature [6-7]. Nevertheless it has many shortcomings in real situations. Indeed, the assessment of the temperature depends on the thermal source generation caused by the current density, the electric field due to Joule effect and the electron carrier mobility attributable to the polar optical phonon scattering. Conversely, the temperature evolution affects the electrical characteristics.

Another advance which may be valid is the Fourier thermal transfer theory. This breakthrough has proven to be suitable for the study of thermal conduction in a large number of electronic components [8-9]. Nevertheless, at the nano-electronics components based HEMTs heterostructure, additional complex phenomena are associated with thermal conduction processes [10]. To study thermal conduction in HEMT-based electronic devices at the nanoscale, the dual-phase-lag theory (DPL) was developed to overcome the weakness of the conventional Fourier thermal transfer theory [11-12]. In order to describe the microscopic electron phonon interactions, the Dual-Phase-Lag thermal conduction model taken into account the two relaxation parameters τ_T (the phase lag of the temperature gradient which trap the time delay ensuing from the microstructural interaction effect) and τ_q (the phase lag of the thermal flux that trap the quick transient effect of thermal inertia) model has been developed by Tzou [13-14].

In this work, we consider the combined dependence between the electronic and thermal characteristics on the nano $Al_xGa_{1-x}N$/GaN HEMTs based electronic devices. In section 2, the DPL equation joined with the Schrödinger-Poisson equations is detailed. In section 3, the discussion results of electrical and thermal characteristics are studied with respect to the Aluminum fraction.

2. Theoretical formulation

2.1. Dual phase lag heat transfer equation

The thermal transfer comportment of nano-electronic devices is expressed by the subsequent equation:

$$\rho C_p \frac{\partial T(z,t)}{\partial t} = -\nabla q(z,t) + Q \tag{1}$$

where ρ, C_p, q and Q are the thermal capacity, the thermal flux and the heat source generation rate, respectively.

The dual phase lag thermal transfer theory associates the thermal flux and the temperature gradient by means of the subsequent law [14]:

$$q(z, t + \tau_q) = -k\nabla T(z, t + \tau_T) \tag{2}$$

Equation (2) can be expressed as a Taylor-series expansion. The first order development allows:

$$q(z,t) + \tau_q \frac{\partial q(z,t)}{\partial t} = -k\left(\nabla T(z,t) + \tau_T \frac{\partial \nabla T(z,t)}{\partial t}\right) \tag{3}$$

Replacing the heat flux $q(z,t)$ into Eq. (1), we achieve the one-dimensional Dual phase lag equation:

$$\frac{\partial T}{\partial t} + \tau_q \frac{\partial^2 T}{\partial t^2} = \tau_T \alpha \frac{\partial}{\partial t}\left(\frac{\partial^2 T}{\partial z^2}\right) + \alpha \frac{\partial^2 T}{\partial z^2} + \frac{\alpha}{k} Q \tag{4}$$

here, $\alpha = k/\rho C_p$ is thermal diffusivity.

The thermal source generation rate Q is principally caused by the Joule heating.

$$Q = \boldsymbol{J} \cdot \boldsymbol{E} \tag{5}$$

where $J(= ne\mu_e(T)E + k_B T\mu_e(T)\frac{\partial n(Z)}{\partial Z})$ is the drift-diffusion current density and $E(= -\nabla E_c(z)/\mathrm{e})$ visualize the electric field.

Temperature and doping dependencies of electron mobility (μ_e) of GaN and AlN is presented as follows [15-16]:

$$\mu^{\Gamma}(T,N) = \mu^{min} + \frac{\mu^{L} - \mu^{min}}{1 + \left(\frac{N}{N^{ref}}\right)^{\gamma_0}} \tag{6}$$

where $\mu^{min} = \mu_{300}^{min}\left(\frac{T}{300K}\right)^{\gamma_1}$, $\mu^{L} = \mu_{300}^{L}\left(\frac{T}{300K}\right)^{\gamma_1}$ and $N^{ref} = N_{300}^{ref}\left(\frac{T}{300K}\right)^{\gamma_2}$

Temperature dependency of the thermal capacity is then evaluated by [17]:

$$C_p^{\Gamma}(T) = C_p^{\Gamma}(300K) + C_1 \frac{\left(\frac{T}{300}\right)^{\gamma} - 1}{\left(\frac{T}{300}\right)^{\gamma} + \frac{C_1}{C_p(300K)}} \tag{7}$$

The boundary and initial conditions are given as follows:

$$\left.\frac{\partial T(z,t)}{\partial z}\right|_{z=0} = \left.\frac{\partial T(z,t)}{\partial z}\right|_{z=L} = 0 \tag{8}$$

$$T(z,0) = T_0 = 300K \text{ and } \frac{\partial T}{\partial t}(z,0) = 0 \text{ for } z \in [0,L] \tag{9}$$

Table 1. The suggested values of thermal diffusivity coefficient used for GaN and AlN [15-16-18].

Parameters	GaN	AlN
$k(\mathrm{W/mK})$	$130(T/300)^{-0.43}$	$350(T/300)^{-1.7}$
$C_p(300K)(Jkg^{-1}K^{-1})$	431	748
C_1	171	482
γ	1.75	2.29
$\rho(300K)(gcm^{-3})$	6.15	3.23
$\mu_{300}^{L}\,(cm^2/Vs)$	1600	683
$\mu_{300}^{min}(cm^2/Vs)$	100	29
$N_{300}^{ref}(10^{17}cm^{-3})$	3	5
γ_0	0.7	0.8
γ_1	-3.7	-3.21
γ_2	-0.2	1.21
γ_3	1.3	-0.18

2.2. Schrödinger-Poisson equations

The electronic characteristics of the HEMTs heterostructure is considered by working out both Schrödinger-Poisson equations [19]:

$$-\frac{\hbar^2}{2}\frac{d}{dz}\left(\frac{1}{m^*(z)}\frac{d\psi_{v,k_z}(z)}{dz}\right) + \Delta E_c(z)\psi_{v,k_z}(\mathrm{AlGaN/GaN}\ z) = E_v\psi_{v,k_z}(z) \tag{10}$$

$$\varepsilon_0\frac{d}{dz}\left(\varepsilon_r(T)\frac{dV_H(T)}{dz}\right) = e^2\left(N_D(z) - n(T)\right) \tag{11}$$

where z, m^*, ΔE_c, ε_r, k_z, E_v and N_D are, respectively, the depth direction, the effective mass of electrons, the conduction band energy, the dielectric constant, the wave vector, the energy subband index and the ionized donors density.

The density of the electrons $n(T)$ is expressed as follows:

$$n(T) = \sum_v \frac{m^*(T)k_BT}{\pi\hbar^2} log\left[1 + \exp\left(\frac{E_F - E_v}{k_BT}\right)\right]\left|\psi_{v,k_z}(T)\right|^2 \quad (12)$$

where E_F is the Fermi energy level and fulfills the neutrality equation:

$$\sum_v \frac{m^*(T)k_BT}{\pi\hbar^2} log\left[1 + \exp\left(\frac{E_F - E_v}{k_BT}\right)\right] - N_D^{2D}\left[1 - \frac{1}{1+\frac{1}{2}\exp\left(\frac{E_D - E_F}{k_BT}\right)}\right] - \frac{\sigma_s}{e} = 0 \quad (13)$$

where $N_D^{2D}(= 210^{12} cm^{-2})$ is the density of dopants and E_D is the binding energy of donors $(= 30$ meV) [20].

The two-dimensional-electron-gas ($n_{2\mathrm{DEG}}$) density is calculated in all subbands as follows:

$$n_{2\mathrm{DEG}}(T) = \sum_v \frac{m^*(T)k_BT}{\pi\hbar^2} log\left[1 + \exp\left(\frac{E_F - E_v}{k_BT}\right)\right] \quad (14)$$

The electron effective mass as a function is illustrated by the equation [21]:

$$\frac{m_0}{m^*(T)} = 1 + \left[\frac{E_P^\Gamma(E_g^\Gamma(T) + (2/3)\Delta_{s0})}{E_g^\Gamma(T)(E_g^\Gamma(T) + \Delta_{s0})}\right] \quad (15)$$

where m_0, Δ_{s0}, E_P^Γ and E_g^Γ are, respectively, the free electron mass, the spin orbit splitting, the energy associated to the momentum matrix element and the band gap energy. The suggested constants utilized in Equation (15) are summarized in Table 2 for GaN and AlN [21].

The temperature dependency of the dielectric constant (ε_r) for GaN and AlGaN as approximated by [22]:

$$\varepsilon_r^{GaN}(T) = 8.9 exp[10^{-4}(T - 300)] \quad (16)$$

$$\varepsilon_r^{Al_xGa_{1-x}N}(T) = \varepsilon_r^{GaN}(T) - 4x \quad (17)$$

The sum potential energy ΔE_c is given as follows:

$$\Delta E_c(T, x) = \Delta E_g(T, x) + V_H(T) + V_{ex}(T) + V_P(T) \quad (18)$$

where ΔE_g, V_H, V_{ex} and $V_P(= eF_z z)$ are, respectively, the heterointerface band gap discontinuity, the effective Hartree potential, the exchange-correlation potential and the potential energy attributable to the polarization charge density in the AlGaN/GaN hetrostructure.

The electric field (F_z) attributable to the spontaneous (SP) and piezoelectric (PZ) polarizations in the barrier and well are given as follows [23]:

$$F_z^{Al_xGa_{1-x}N} = \frac{\left|P_{GaN}^{PZ} - P_{Al_xGa_{1-x}N}^{SP} - P_{Al_xGa_{1-x}Nw}^{PZ}\right|}{\varepsilon_0 \varepsilon_r^{Al_xGa_{1-x}N} + \varepsilon_0 \varepsilon_r^{GaN}\left(\frac{L_{Al_xGa_{1-x}N}}{L_{GaN}}\right)} \tag{19}$$

$$F_z^{GaN} \to 0 \tag{20}$$

where ($L_{Al_xGa_{1-x}N}$) and (L_{GaN}) correspond to the barrier and well layers.

The polarization charge density at the heterointerfaces is given as follows [24]:

$$P_{Al_xGa_{1-x}N}^{sp} = -0.09x - 0.034(1-x) + 0.021x(1-x) \tag{21}$$

$$P_{AlN}^{pz} = -1.808\varepsilon - 7.888\varepsilon^2 \tag{22}$$

$$P_{GaN}^{pz} = -0.918\varepsilon + 9.541\varepsilon^2 \tag{23}$$

$$P_{GaN}^{sp} = -0.029$$

The basal strain (ε) is exhibited as a function of the lattice constant of the substrate (a_s) and the epilayer (a_e):

$$\varepsilon(T,x) = \frac{a_s(T) - a_e(T,x)}{a_e(T,x)} \tag{24}$$

The temperature dependencies of the lattice constants are expressed as:

$$a_e(T,x) = a_0(x)[1 + \beta(T - 300)] \tag{25}$$

$$a_s(T) = 0.32[1 + \beta(T - 300)] \tag{26}$$

where β is the coefficient of thermal expansion.

The equilibrium lattice constant (a_0) with respect to the aluminum fraction is given as follows [25]:

$$a_0(x) = 0.31986 - 0.00891\,x \tag{27}$$

The piezoelectric polarization of $Al_xGa_{1-x}N$ is expressed by Vergard's law as

$$P_{Al_xGa_{1-x}N}^{pz} = xP_{AlN}^{pz} + (1-x)P_{GaN}^{pz} \tag{28}$$

The sum of polarization at the heterointerface is evaluated as:

$$\sigma_s = \left|P_{Al_xGa_{1-x}N}^{sp} + P_{Al_xGa_{1-x}N}^{pz} - P_{GaN}^{sp}\right| \tag{29}$$

The exchange-correlation potential is expressed as [26]:

$$V_{ex}(T) = -0.916\frac{e^2}{6\pi\varepsilon_0\varepsilon_r(T)}\left[\frac{3n(T)}{4\pi}\right]^{1/3} \quad (30)$$

The conduction band offset energy (ΔE_g) of the AlGaN/GaN heterointerface is expressed as:

$$\Delta E_g(T,x) = 0.75\left[E_g(\text{top}) - E_g(\text{bottom})\right] \quad (31)$$

where $E_g(\text{top})$ and $E_g(\text{bottom})$ are the band gaps of the top/bottom layers sides of the heterointerface. The band gap of $Al_xGa_{1-x}N$ as a function of both the temperature and the Aluminum fraction is expressed by means of Varshni's law:

$$E_g^{Al_xGa_{1-x}N}(T,x) = xE_g^{AlN}(T) + (1-x)E_g^{GaN}(T) - 0.6x(1-x) \quad (32)$$

The temperature dependencies of the band gap energy of the AlN and GaN are given by [27].

$$E_g^{AlN}(T) = E_g^{AlN}(T=0K) - \frac{1.18\,10^{-3}T^2}{T+1462} \quad (33)$$

and

$$E_g^{GaN}(T) = E_g^{GaN}(T=0K) - \frac{0.909\,10^{-3}T^2}{T+800} \quad (34)$$

TABLE 2. The recapitulated parameters used for GaN and AlN [21] [28].

Parameters	GaN	AlN
$E_P^{\Gamma}(\text{eV})$	14.0	14.5
$E_g^{\Gamma}(0K)(eV)$	3.42	6.23
$\Delta_{s0}(eV)$	0.014	0.019
$\beta(10^{-6}K^{-1})$	5.59	4.2

3. Results and discussion

To illustrate this approach, the electrical characteristic of the AlGaN/ GaN HEMT heterostructure on G-face configuration is considered. Figure 1 illustrates a cross-section illustration of the AlGaN/GaN HEMT with a depth of 20 nm in the AlGaN quantum barrier and a depth of 30 nm in the GaN quantum well. The doping concentration in the upper AlGaN layer and the lower GaN layer are, respectively, $N_A = 2\text{x}10^{17}\text{cm}^{-3}$ and $N_D = 2\text{x}10^{18}\text{cm}^{-3}$. The Aluminum fraction x was set to 20-30%. The phase lag of the heat flux is $\tau_q = 8.5\,ps$ and the phase lag of the temperature gradient is $\tau_T = 90\,ps$. The bias voltage is estimated by

voltage sweeps across the device in the range of 0 eV to 1.2 eV. In fact, the comportment of the electronic and thermal quantities as a function of the Aluminum fraction (x=0.2, 0.25 and 0.3) is investigated.

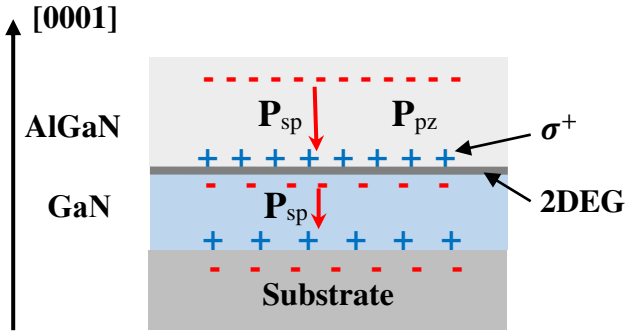

Figure 1. Cross-section illustration of the AlGaN/GaN HEMT on G-face configuration.

Figure 1 also shows the spontaneous polarization (P_{sp}) and piezoelectric polarization (P_{pz}) vectors and the charges in G-face configuration. Herein illustration, the AlGaN/GaN heterointerface is then under compressive surface stress because the lattice constants of the GaN sheet are lesser than those of the AlGaN sheet. Therefore, a positive density charge and an electric field within an AlGaN/GaN heterointerface are obtained. This density is remunerated by the occupancy of the two-dimensional electron gas density (2DEG).

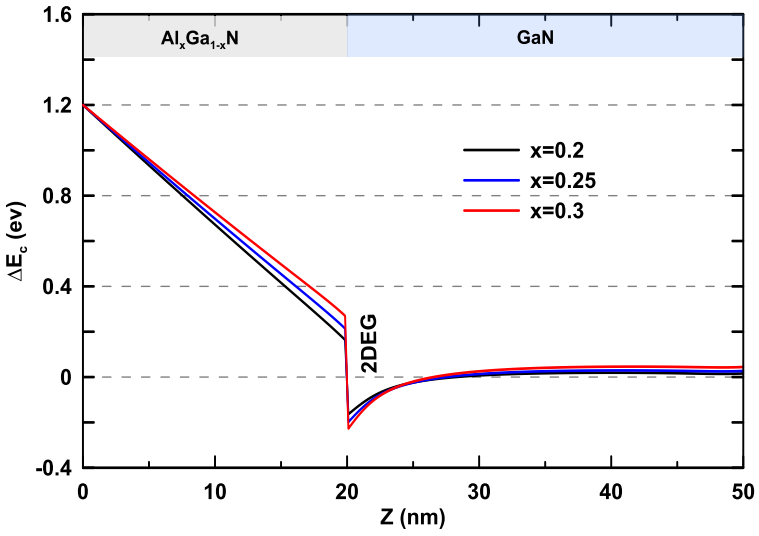

Figure 2. The conduction-band edge potential (ΔE_c) vs. the depth z with three values of Aluminum fraction (x=0.2, 0.25 and 0.3).

In Figure 2, the conduction-band edge potential (ΔE_c) for different values of Aluminum fraction (x=0.2, 0.25 and 0.3) is offered. It is noticeable that the ΔE_c has at a triangular shape within the AlGaN/GaN heterointerface. It is also shown that the curve becomes deeper with the higher Aluminum fraction. This is chiefly attributable to the internal quantum-confined Stark effect which increases with the increases of Aluminum fraction [26]. Additionally, the disagreement in piezoelectric and spontaneous polarizations between the AlGaN and the GaN layers induced the formation of a 2DEG density in the heterointerface. Furthermore, Figure 2 shows that the conduction-band offset ΔE_g is enlarged relatively to the Aluminum fraction. Within the cases considered in this study and at $t = 100\,ps$, the conduction-band offset of the AlGaN/GaN HEMT enlarged from 0.34eV to 0.52eV when x increased from x=0.2 to x=0.3.

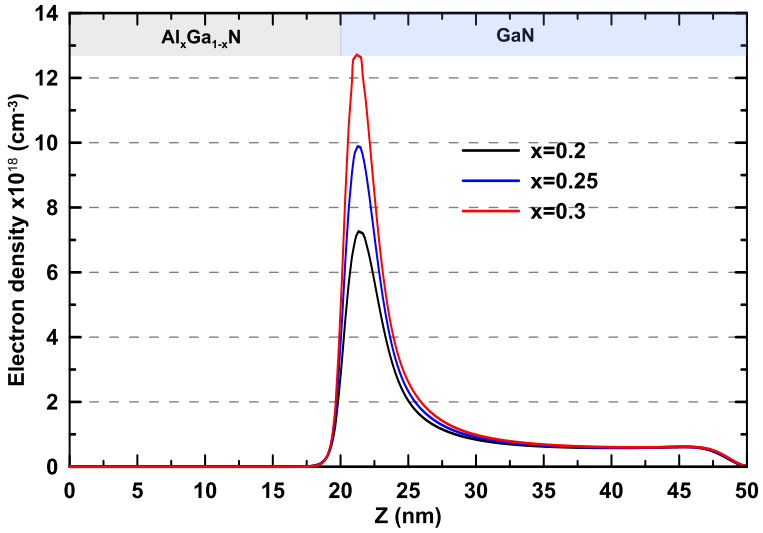

Figure 3. The density of electron vs. the depth z with three values of Aluminum fraction (x=0.2, 0.25 and 0.3).

Figure 3 presents the density of electron as a function of the depth z with diverse values of Aluminum fraction and at $t = 100\,ps$. It is shown that the entire distribution reached a maximum in the surrounding area of the heterointerface and deflated once moved away. The GaN thin sheet is further occupied by the electron with the increase of the Aluminum fraction. Therefore, the maximum of the electron density (n_{max}) rose with the growth of Aluminum fraction from 7.26×10^{18} to 12.72×10^{18}cm^{-3} respectively with x=0.2 and x=0.3. Accordingly, an increase in the two-dimensional-electron gaz density (n_{2DEG}) from 1.12×10^{14} to 1.19×10^{12} cm^{-2} respectively with x=0.2 and x=0.3.

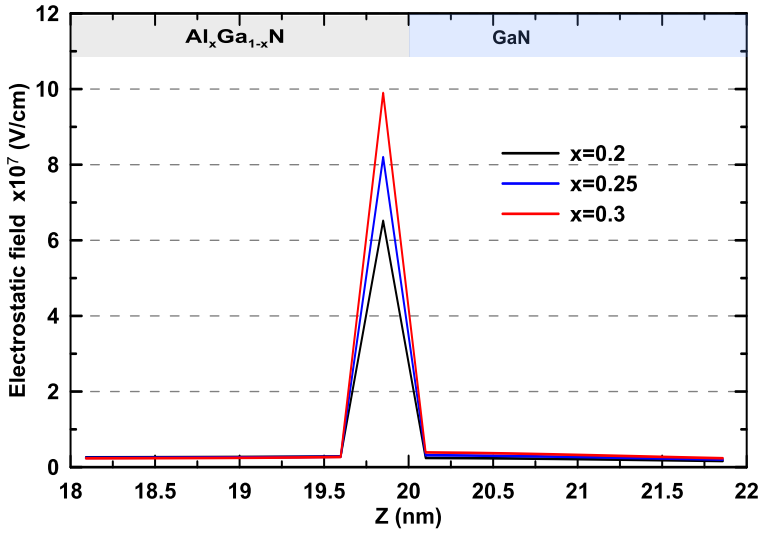

Figure 4. The electrostatic field vs. the depth z with three values of Aluminum fraction (x=0.2, 0.25 and 0.3).

Figure 4 shows the electrostatic field as a function of the depth z with several values of Aluminum fraction and at $t = 100\,ps$. It is shown that the electric field is significant in the surrounding area of the heterointerfaces. Additionally, it intensified whith the growth of Aluminum fraction. This phenomenon is interpreted by the distended energy band diagrams presented in Fig. 2. The value of the maximum electrostatic field in the $Al_xGa_{1-x}N$/GaN heterointerface shows an increase from 6.51 10^7 V/cm at x=0.2 to 9.89 10^7 V/cm at x=0.3.

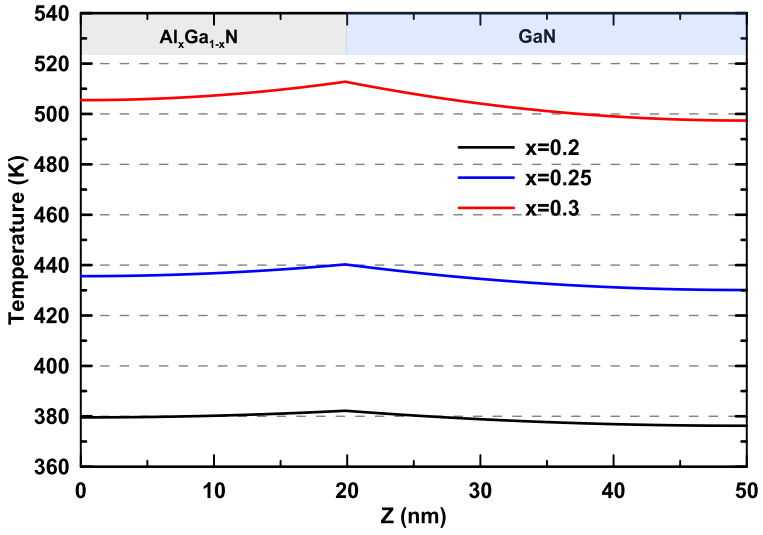

Figure 5. The temperature distribution vs. the depth z with three values of Aluminum fraction (x=0.2, 0.25 and 0.3).

Figure 5 displays the temperature distribution versus the depth z for several values of Aluminum fraction. It is shown that the temperature grew remarkably with the growth of

Aluminum fraction from x=0.2 to x=0.3. For an each value of the Aluminum fraction, the temperature distribution reached a peak in the vicinity of the AlGaN/GaN heterointerface and deflated when one moves away. This is mainly caused by the higher polarization impact and the higher density of electron occupations in the triangular shape. Therefore, the maximum temperature, at $t = 100\ ps$, increased by 34% (from 382.2 K to 512.8 K, respectively). Based on the thermal dissipation efficiency η ($= (T_d - T_0)/T_0$), where T_d and T_0 is the highest temperature in the AlGaN/GaN HEMT heterostructure with and without a thermal dissipation, respectively. It follows that when the aluminum fraction remained relatively high the efficiency of the thermal dissipation displayed a sharp growth. Thus, for example, the efficiency soared by 150 % (from 28 % to 72 %) at $t = 100ps$ when the Aluminum fraction was changed from 0.2 to 0.3.

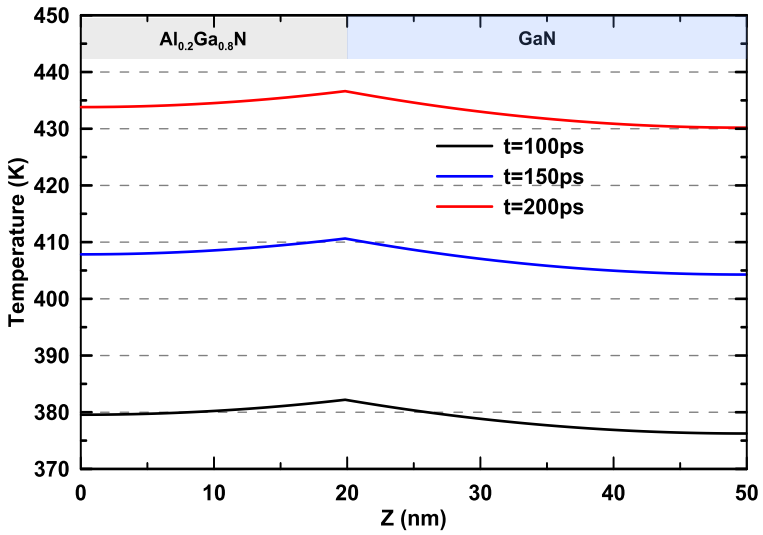

Figure 6. Temperature variation vs. the depth z at a range of times (t=100, 150 and 200ps).

Figure 6 presents the temperature variation as a function of the depth z for Aluminum fraction x=0.2 at various times (t=100, 150 and 200ps). It is revealed that temperature variation increased remarkably along with the time from t=100ps to t=200ps. Therefore, the maximum temperature increases by 12% from 100, to 200ps. The similar trend of temperature increase versus the times was revealed in AlGaN/GaN HEMT-based heterostructure in [29-31]. However, the thermal source due principally to the Joule dissipation result in addition seeing that phonon wall collisions. In addition, the increase of the Aluminum fraction shows an increase of the polarization charge and therefore the amplification of the electrostatic field.

Given that the thermal source generation depends on the electrostatic field, the temperature variation grew along with the Aluminum fraction.

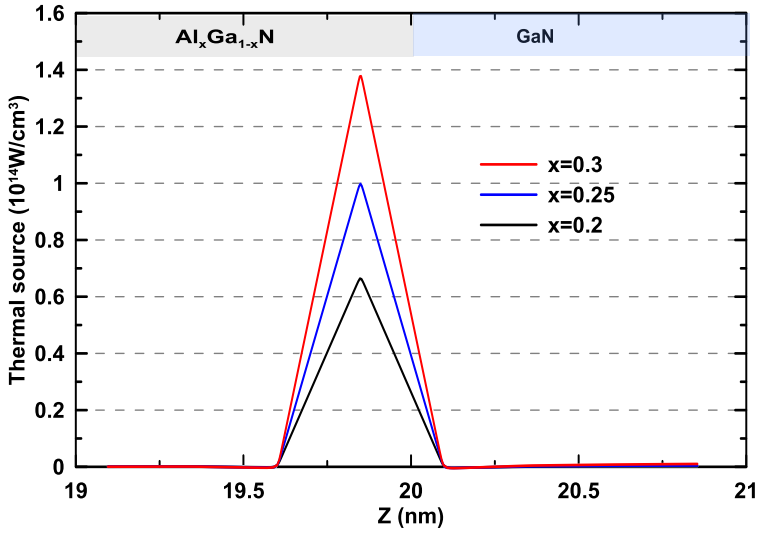

Figure 7. The thermal source variation vs. the depth z with three values of Aluminum fraction (x=0.2, 0.25 and 0.3).

Figure 7 shows the thermal source generation versus the depth z for several values of Aluminum fraction and at $t = 100\,ps$. At the heterointerface of AlGaN/GaN, the thermal generation process reached a highest peak. This is caused by the occupancy of the electron density and the highs electrical field. This confirms the suggestion of the consequence of the subband occupation of the two-dimensional electron gas at the AlGaN/GaN heterointerface. The calculated value of the thermal source generation in the AlGaN/GaN heterointerface shows an increase from 0.66×10^{14}W/cm^3 at x=0.2 to 1.38×10^{14}W/cm^3 at x=0.3.

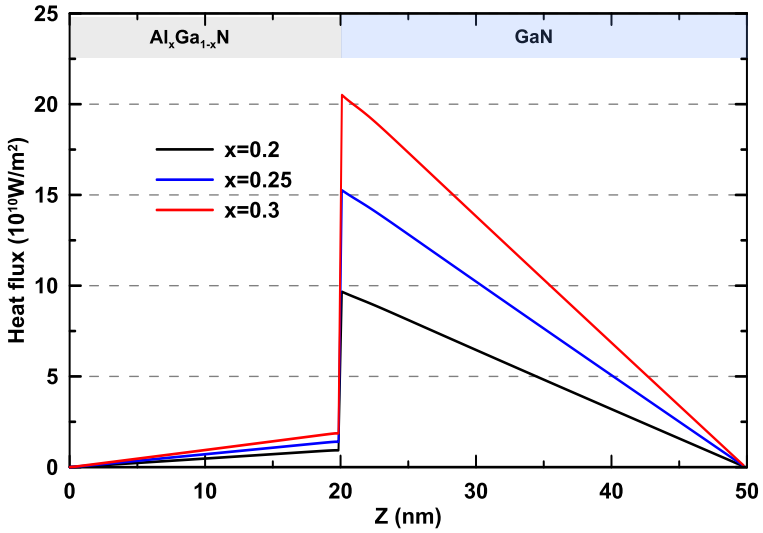

Figure 8. The thermal flux variation vs. the depth z with three values of Aluminum fraction (x=0.2, 0.25 and 0.3).

Figure 8 displays the variation of thermal flux versus the depth z for several values of Aluminum fraction and at $t = 100\,ps$. It is shown that the thermal flux enhanced versus the Aluminum fraction. Nevertheless, the increase in the triangular quantum shape is caused by the enhancement of the thermal conductivity of GaN as compared to that of AlGaN. The thermal flux in such case has a peak at the AlGaN/GaN heterointerface. It is clear that, when the Aluminum fraction x grew from 0.2 to 0.3, the peak value of the thermal flux grew from 9.66×10^{10}W/m^2 to 20.5×10^{10}W/m^2 respectively.

4. Conclusion

The AlGaN/GaN HEMTs could advance high power-efficient nano-electronic devices. That's why it deserves crucial to expand a model to truthfully explain the thermal transfer impacts in nano-electronics devices, which considerably have an effect on the performance of the electrical characteristics. The present model coupled with the Schrödinger-Poisson and the dual phase lag thermal transfer equations has been evaluated to simulate the AlGaN/GaN HEMTs. The spontaneous and piezoelectric polarization field effect together conduction band offset effect between the AlGaN/GaN heterointerface leads to the formation of the 2DEG density. Moreover, it is shown that the 2DEG density increases with the increase of the Aluminum fraction. In addition, the simulated result of the thermalization process was found to be in good agreement with literature. In view of that, the temperature, the thermal source generation and the thermal flux grow at the heterointerface with the growth of the Aluminum

fraction. The result was found to be useful in assessing thermal transfer in the AlGaN/GaN HEMTs nano-devices to improve their performance.

Conflict of Interest: The authors declare that they have no conflict of interest

5. References

[1] Tang Y, Shinohara K, Regan D, Corrion A, Brown D, Wong J, Schmitz A, Fung H, Kim S, Micovic M (2015) Ultrahigh-Speed GaN High-Electron-Mobility Transistors With fT/fmax of 454/444 GHz. IEEE Electron Device Letters 36(6):549-551

[2] Harvard E, Brown R, Shealy JR (2011) Performance of AlGaN/GaN high-electron mobility transistors with AlSiN passivation. IEEE Transactions on Electron Devices 58(1):87-93

[3] Wang A, Tadjer MJ, Calle F (2013) Simulation of thermal management in AlGaN/GaN HEMTs with integrated diamond heat spreaders. Semiconductor science and technology 28:1-8

[4] Altuntas P, Lecourt F, Cutivet A, Defrance N, Okada E, Lesecq M, Rennesson S, Agboton A, Cordier Y, Hoel V, DeJaeger JC (2015) Power performance at 40Ghz of AlGaN/GaN High-Electron Mobility Transistors Grown by Molecular Beam Epitaxy on si(111) Substrate. IEEE Electron Device Letters 34:490–492

[5] Sharma CS, Tiwari MK, Michel B, Poulikakos D (2013) Thermofluidics and energetics of a manifold microchannel heat sink for electronics with recovered hot water as working fluid. International Journal of heat Mass Transfer 58:135-151

[6] Polash BA, Huq H (2008) High temperature performance measurement and analysis of GaN HEMTs. Proceedings of the Society of Photo-Optical Instrumentation Engineers (SPIE) 6894.

[7] Darwish AM, Huebschman BD, Viveiros E, Hung HA (2009) Dependence of GaN HEMT millimeter-wave performance on temperature. IEEE Transactions on Microwave Theory and Techniques 57(12):3205–3211

[8] Wachutka GK (1990) Rigorous thermodynamic treatment of heat generation and conduction in semiconductor device modeling. IEEE Transactions on Computer-Aided Design of Integrated Circuits and Systems 9:1141-1149

[9] Yang L, Ai S, Chen Y, Cao M, Zhang K, Ma X, Hao Y (2013) A self-heating study on multi-finger AlGaN/GaN high electron mobility transistors. Journal of Semiconductors 34:074005

[10] Ordonez-Miranda J, Alvarado-Gil JJ (2011) On the stability of the exact solutions of the dual-phase lagging model of heat conduction. Nanoscale Research Letters, 6:327

[11] Nasri F, Ben Aissa MF, Belmabrouk H (2017) Nonlinear Electrothermal Model for Investigation of Heat Transfer Process in a 22-nm FD-SOI MOSFET, IEEE Trans. Electron Dev., 64 (4) 1461-1466.

[12] Cheng AQ, Ding DZ, Zeng H, Chen RS, (2018) Transient Analysis for Electrothermal Properties in Nanoscale Transistors, IEEE Trans. Electron Dev., 65 (9), 3930-3935.

[13] Tzou DY (1995) A unified field approach for heat conduction from macro- to microscales. J. Heat Transfer (ASME) 117:8–16

[14] Tzou DY (1996) Macro-To Micro-Scale Heat Transfer: The Lagging Behavior. Taylor & Francis, Washington

[15] Vitanov S, Palankovski V, Maroldt S, Quay R (2010) High-Temperature Modeling of AlGaN/GaN HEMTs. Solid-State Electron 54(10):1105-1112

[16] Adachi S (2007) Lattice thermal conductivity of group-IV and III–V semiconductor alloys. J. Appl. Phys 102(6):063502

[17] Palankovski V, Schultheis R, Selberherr S, (2001) Simulation of Power Heterojunction Bipolar Transistors on Gallium Arsenide. IEEE Trans.Electron Devices 48(6):1264-1269

[18] Palankovski V, Quay R (2004) Analysis and Simulation of Heterostructure Devices. Wien, New York: Springer

[19] Gazzah MH, Chouchen B, Fargi A, Belmabrouk H (2019) Electro-thermal modeling for InxGa1-xN/GaN based quantum well heterostructures. Materials Science in Semiconductor Processing 93:231-237

[20] Chu RM, Zhou YG, Zheng YD, Han P, Shen B, Gu SL (2001) Influence of doping on the two-dimensional electron gas distribution in AlGaN/GaN heterostructure transistors. Appl. Phys. Lett. 79:2270

[21] I. Vurgaftman, J.R. Meyer, L.R. Ram-Mohan, (2001) Band parameters for III–V compound semiconductors and their alloys. J. of Applied Physics 89:5815-5875

[22] A.M. Elabsy, (1994) Effect of the Gamma -X crossover on the binding energies of confined donors in single GaAs/$Al_xGa_{1-x}As$ quantum-well microstructures. J. Phys. Condens. Matter 6(46):10025-10030

[23] S.H. Park, (2001) Spontaneous Polarization Effects on Electronic and Optical Properties of Wurtzite GaN/AlGaN Quantum Well Lasers. J. Korean Phys. Soc., 38(4):420-426

[24] Ambacher O, Majewski J, Miskys C, Link A, Hermann M, Eickhoff M, Stutzmann M, Bernardini F, Fiorentini V, Tilak V, Schaff B, Eastman LF (2002) Pyroelectric properties of Al(In)GaN/GaN hetero- and quantum well structures. Journal of Physics: Condensed Matter, 14:3399

[25] Zhang JF, Zhang JC, Hao Y (2004) Temperature dependence of Hall electron density of GaN-based heterostructures, J. Chin. Phys 13(8):1334-1338.

[26] Ben Jazia A, Mejri H, Maaref H, Souissi K (1997) Stark effect studied in δ-doped GaAs structures. Semiconductor Science and Technology 12(11):1388

[27] Christensen NE, Gorczyca I (1994) Optical and structural properties of III-V nitrides under pressure. Phys. Rev. B 50:4397-4415

[28] Piprek J (2007) Nitride Semiconductor Devices.Weinheim: Wiley

[29] Jones JP, Rosenberger MR, King WP, Vetury R, Heller E, Dorsey D, Graham S (2014) Electro-thermo-mechanical transient modeling of stress development in AlGaN/GaN high electron mobility transistors (HEMTs), 14th IEEE ITHERM Conference, Orlando, FL, USA

[30] Menozzi R, Cova P, Delmonte N, Giuliani F, Sozzi G (2015) Thermal and electro-thermal modeling of components and systems: A review of the research at the University of Parma Facta universitatis-series: Electronics and Energetics 28(3):325-344

[31] Arivazhagan L, Nirmal D, Ajayan J, Godfrey D, Rakkumar JS, Bhagya Lakshmi S (2019) Modeling of Self-Heating for AlGaN/GaN HEMT with Thermal Conductivity Degradation Effect. AIP Conference Proceedings 2201:020010

Figures

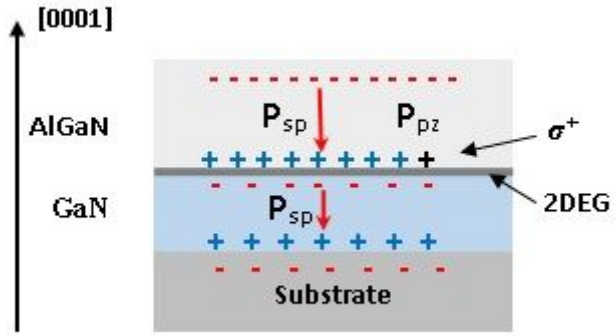

Figure 1

Cross-section illustration of the AlGaN/GaN HEMT on G-face configuration.

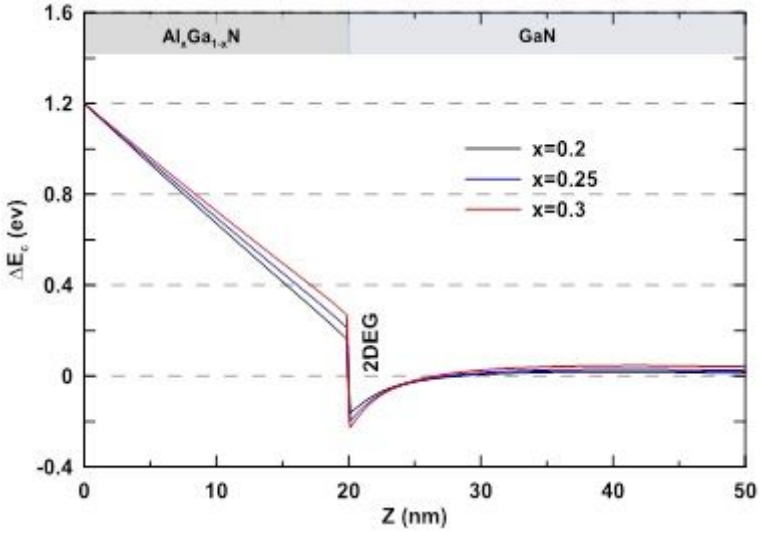

Figure 2

The conduction-band edge potential (AEc) vs. the depth z with three values of Aluminum fraction (x=0.2, 0.25 and 0.3).

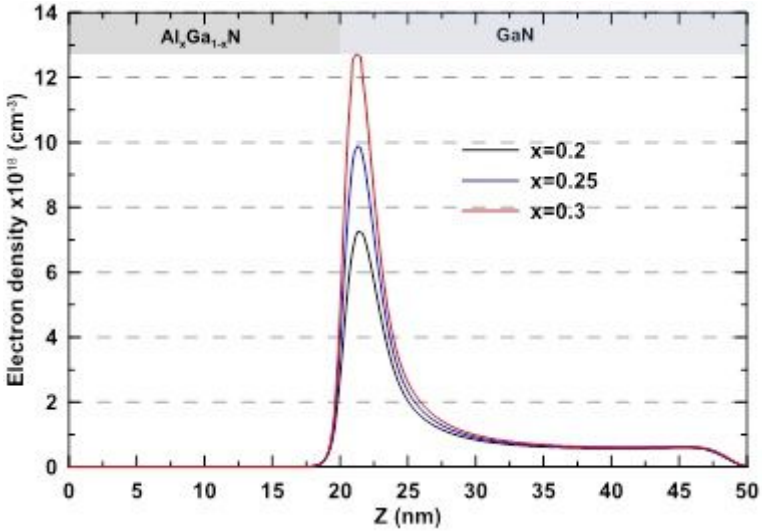

Figure 3

The density of electron vs. the depth z with three values of Aluminum fraction (x=0.2, 0.25 and 0.3).

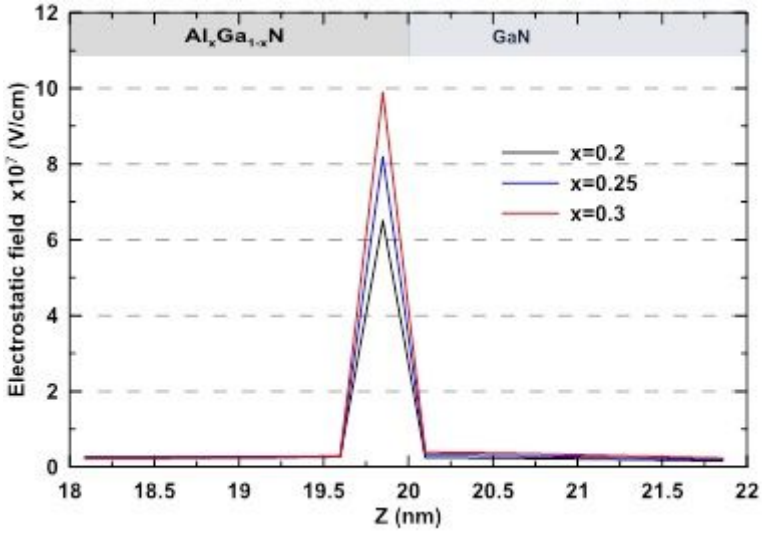

Figure 4

The electrostatic field vs. the depth z with three values of Aluminum fraction (x=0.2, 0.25 and 0.3).

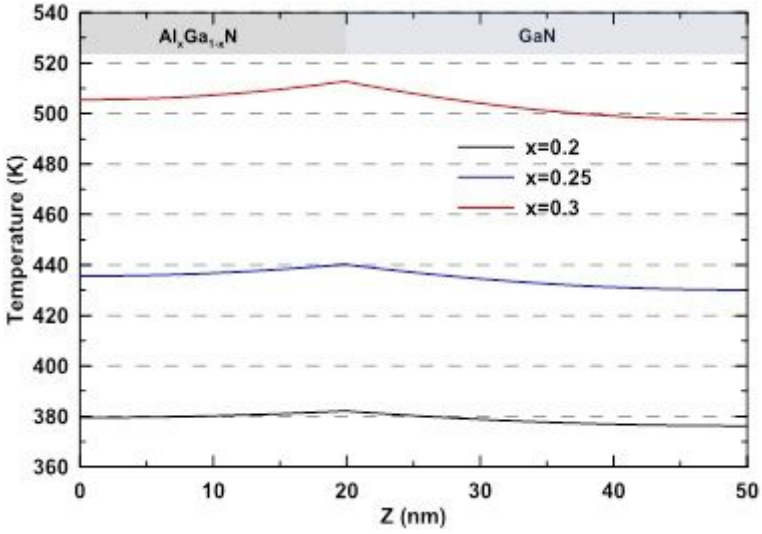

Figure 5

The temperature distribution vs. the depth z with three values of Aluminum fraction (x=0.2, 0.25 and 0.3).

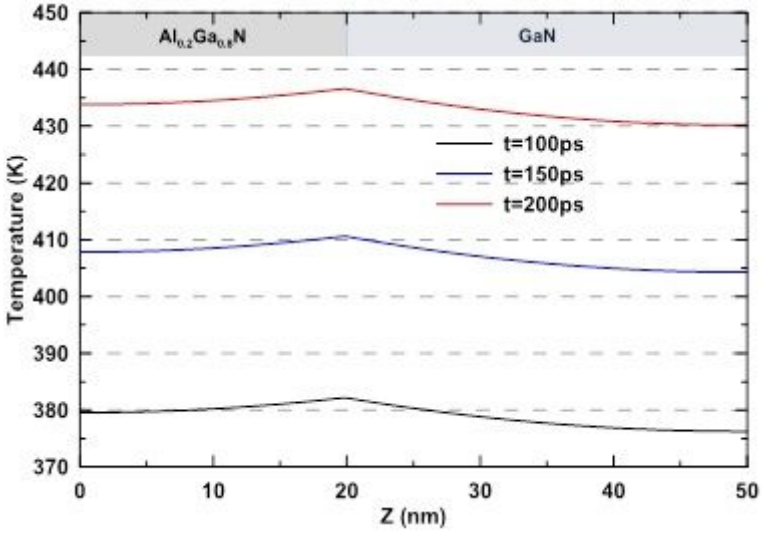

Figure 6

Temperature variation vs. the depth z at a range of times (t=100, 150 and 200ps).

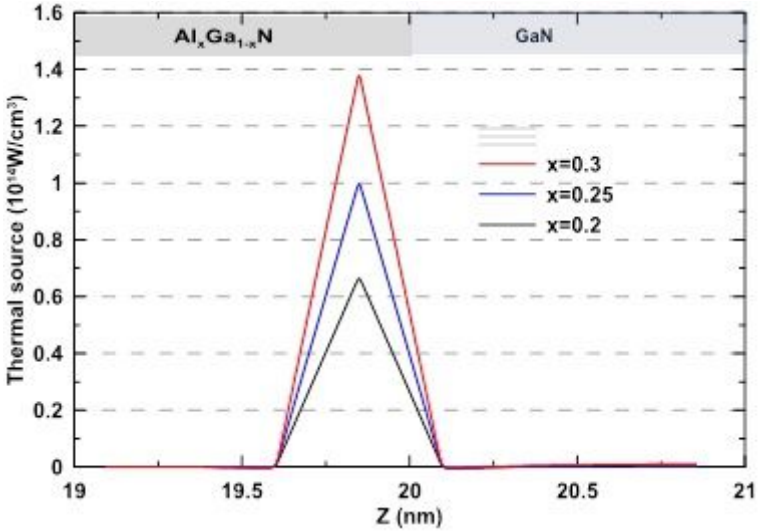

Figure 7

The thermal source variation vs. the depth z with three values of Aluminum fraction (x=0.2, 0.25 and 0.3).

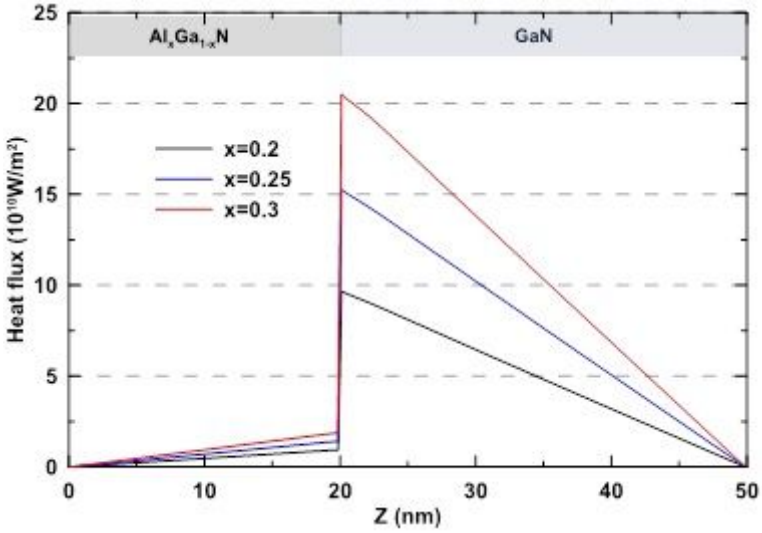

Figure 8

The thermal flux variation vs. the depth z with three values of Aluminum fraction (x=0.2, 0.25 and 0.3).